Type-II $InAs_xSb_{1-x}$/InAs quantum dots for midinfrared applications: Effect of morphology and composition on electronic and optical properties

G. H. Yeap,* S. I. Rybchenko, I. E. Itskevich, and S. K. Haywood
Department of Engineering, University of Hull, Hull, HU6 7RX, United Kingdom
(Received 12 November 2008; published 9 February 2009)

InSb-based self-assembled quantum dots are very promising for the midinfrared (3–5 μm) optical range. We have analyzed the effect of geometry and composition on the electronic structure and optical spectra of $InAs_xSb_{1-x}$/InAs dots. The calculated transition energies agree well with the available experimental data. The results show that the geometry of the dot can be estimated from the optical spectra if the composition is known, and vice versa.

DOI: 10.1103/PhysRevB.79.075305 PACS number(s): 73.22.Dj, 73.21.La, 78.67.Hc

I. INTRODUCTION

Self-assembled quantum dots (SAQDs) promise a new generation of novel optoelectronic devices. Most of the studies so far have concentrated on the InAs/GaAs system, which is of interest for applications in the near-infrared range. However, midinfrared (MIR) optoelectronic devices are key elements for various applications, such as medical diagnostics, environmental sensing, military countermeasures, etc. In particular, the 3–5 μm atmospheric transmission window is the region of choice for device development due to low CO_2 and H_2O absorption. For this range, InSb-based SAQDs might look most promising because the band gap in bulk InSb is the smallest among III–V semiconductors (0.18 eV at 300 K). However, due to the lattice misfit, which is inherent to Stranski-Krastanov growth of SAQDs, the dots are compressively strained. This increases the direct band gap in type-I InSb dots beyond the 3–5 μm range as has been shown in previous band-structure modeling.[1–3] Hence, for use in MIR devices, alternative SAQD designs need to be considered.

SAQDs with type-II band alignment offer the possibility of optical transitions within the MIR range (albeit with lower quantum efficiency than type-I systems), similar to W-type quantum-well structures.[4] In particular this can be realized for the InSb/InAs SAQD system with an expected type-II broken-gap band alignment. Recently, successful growth of InSb/InAs QDs has been reported,[5–7] with intense photoluminescence (PL) in the 3.9–4.2 μm wavelength range. However, measurement of structural parameters for these dots, such as composition, size, and shape, is very difficult because of their small size (2.5–3 nm). Therefore, it is important to be able to evaluate these parameters from investigation of the electronic structure by optical and transport methods. Accompanying theoretical analysis of the effect of the structural parameters on the electronic and optical properties is also crucial. At the moment, there is a clear deficiency of theoretical modeling for this SAQD system. In particular, the interplay between the structural and electronic properties has not been investigated.

In this paper, we present results from modeling of the electronic and optical properties of $InAs_xSb_{1-x}$/InAs SAQDs, focusing on the effects of SAQD morphology and composition. In particular, we analyze the electronic structure of $InAs_xSb_{1-x}$/InAs SAQD of various shapes, aspect ratios, and compositions. We also suggest a method of assessing the geometry and composition of $InAs_xSb_{1-x}$/InAs quantum dots (QDs) using their optical spectra and limited microscopy information.

This paper is organized as follows. In Sec. II, we describe our calculation methods. In Sec. III A, we analyze the effect of strain, geometry, and composition of the dots on the confinement potential for electrons and holes. In Sec. III B, we analyze the electronic structure of the dots and relate them to the available experimental data. Conclusions are presented in Sec. IV.

II. CALCULATION METHODOLOGY

The actual shape of $InAs_xSb_{1-x}$/InAs SAQDs is unknown. However, we have shown earlier[8] that the governing geometric parameter of a SAQD is the aspect ratio (AR), as defined in Fig. 1. In particular, we have shown that the approximation using a simple ellipsoidal shape is sufficient to reveal the major features of the electronic structure of the dots. In this paper, we examine two shapes: an oblate ellipsoid and a lens. The only variable parameter for both shapes is the AR. We examine the most important effects of the dot structure on the electronic properties for the ellipsoidal shape and then perform the analysis for the lens shape for comparison.

The existence of developed wetting layer in the $InAs_xSb_{1-x}$/InAs SAQD system is still doubtful;[7] because of this, we do not include a wetting layer in our modeling. The piezoelectric potential is not included either because it is expected to be negligible for the dot sizes considered. The material parameters were taken from Ref. 9. Also following

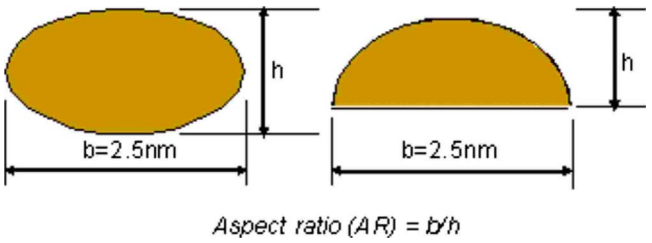

FIG. 1. (Color online) Definition of the aspect ratio (AR).

Ref. 9, all energy values in our paper are given with respect to the valence-band edge in unstrained InSb.

We start by obtaining the strain distribution in the dot and the surrounding matrix in the continuum-elasticity approximation. Both the cubic anisotropy and different elastic constants for the dot and matrix materials are taken into account. We use the finite-element method (FEM) employing commercial COMSOL MULTIPHYSICS software.

Various techniques had been used for studying the strain fields in SAQDs and the surrounding matrix. They range from an analytical continuum approach based on Eshelby's inclusion theory[8,10] to atomistic approach utilizing valence force field model with Keating potential.[11–14] For numerical approaches based on the continuum-elasticity approximation, both the finite difference method[15,16] and the FEM (Refs. 8 and 17–21) have been used. Previous studies have shown that the continuum-elasticity approximation is applicable at the nanoscale even though it was developed for macroscopic structures. The modeling results compare well with the data obtained from transmission electron microscopy (TEM) imaging.[22,23] The flexibility of FEM meshing enables us to analyze SAQDs of arbitrary shape and material composition with acceptable computational cost.

Once the strain components are obtained, the strain-modified profile for the conduction and valence bands is obtained within the standard deformation-potential theory.[8,24] More details of calculations are available in Ref. 8.

The electronic structure is calculated by decoupling the conduction and valence bands, and neglecting the exciton binding energy. The size-quantization energy for holes is calculated using the six-band $\boldsymbol{k}\cdot\boldsymbol{p}$ method.[25–27] The energies of the electron levels are calculated using a single-band effective-mass approach[28–31] with the effect of the band-gap change on the electron effective mass taken into account.

Calculations were performed for two temperatures, 80 and 300 K, to facilitate comparison with experimental data from the literature.[5,6]

III. RESULTS AND DISCUSSIONS

A. Strain and strain-modified band profile

In this section, we analyze the strain distribution and the resulting confinement potential for ellipsoid- and lens-shaped $InAs_xSb_{1-x}$/InAs SAQDs of various ARs and compositions. We start by examining the simplest example of a spherical dot (i.e., ellipsoid of AR=1). Next we examine the effect of increasing AR and compare this with similar calculations for the more complicated lens shape. Note that for both shapes, the strain distribution and the confinement potential are size independent within the approximation used.

The strain within the spherical dot is purely hydrostatic and homogeneous. Hence, the positions of the edges of conduction and valence bands in the dot are well defined. Meanwhile, there is a shear component of strain present in the matrix, which is largest at the dot-matrix interface.

Figure 2(a) shows the unstrained band profile (i.e., if we could somehow turn off the strain) for a spherical InSb/InAs QD. It demonstrates a type-II broken-gap band alignment with a confinement energy of ≈600 meV for degenerate valence bands. Figure 2(b) shows how the band profile is modified by strain. As one can see, the type-II broken-gap band alignment still holds but the band profile changes considerably. The conduction-band edge in the dot shifts to higher energy. This illustrates the dominant effect of the hydrostatic strain which is an increase in the direct band gap. In addition, shallow potential wells for electrons in the InAs matrix arise close to the interface [marked by dashed ellipses in Fig. 2(b)]. This occurs due to the band bending, which does not exist in the unstrained band profile.

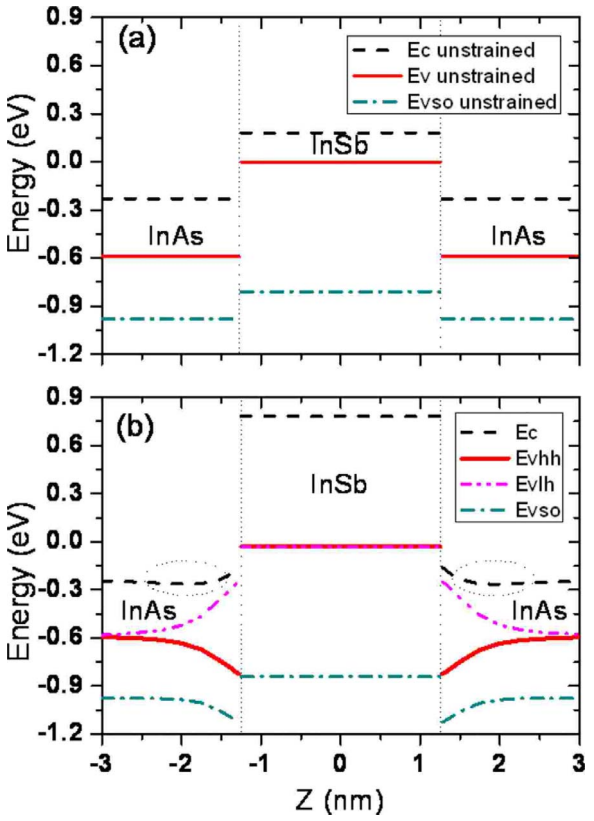

FIG. 2. (Color online) Band profile for spherical InSb/InAs QD along [001] (growth) direction at 80 K: (a) unstrained and (b) strain-modified. Dashed line—conduction band; thin solid line [in (a)]—degenerate valence band; thick solid line [in (b)]—heavy-hole band; dash-dot-dot line—light-hole band; dash-dot line—split-off band. Two dotted ellipses indicate areas of shallow confinement for electrons.

Inside a spherical SAQD, the valence bands are still degenerate. However, shear strain splits the valence bands in the matrix into heavy- and light-hole bands. One can see that strong confinement exists for both heavy and light holes. However, the band bending is of opposite sign for heavy holes and light holes. Hence the confinement potential for heavy holes increases to ≈800 meV. Meanwhile, the confinement potential for light holes does not exceed 600 meV (i.e., the value for the unstrained profile) and it broadens into the matrix region.

A more detailed picture of the strain-modified band profiles can be obtained using two-dimensional cross-section plots. Figure 3 shows these color plots of the band profiles for InSb/InAs SAQDs of ellipsoidal and lens shapes for sev-

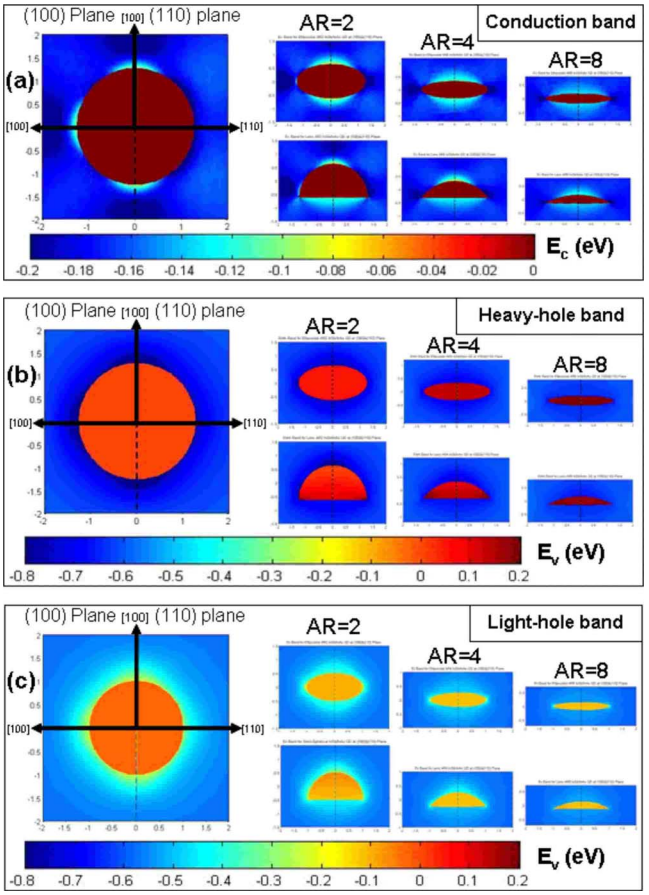

FIG. 3. (Color online) Strain-modified band profile for InSb/InAs QDs of ellipsoidal and lens shapes for several aspect ratios. Each graph shows (100) and (−110) cross-section planes through the dot center on the left- and right-hand-side parts, respectively. (a) Conduction band; (b) heavy-hole band; (c) light-hole band.

eral ARs. Profiles for the conduction band and the heavy- and light-hole valence bands are shown. Each color plot presents the (100) plane on the left and the (−110) plane on the right. The color scale indicates the energy levels in eV. Note that the color scale is the same for heavy- and light-hole bands but it is different for the conduction band.

Figure 3(a) shows the profile for the conduction band. Homogeneous color within the ellipsoidal dots indicates constant energy. (The energy varies slightly within the lens-shape dots). In the matrix, one can see darker blue areas which are most prominent in the (100) plane and for lower ARs. These areas of very shallow confinement potential, which are highlighted by the dotted ellipses in Fig. 2, provide only weak confinement for the electrons. Otherwise, the effects of the shape and AR on the conduction band are minor. The same is true for other possible dot shapes such as the truncated cone or pyramid as it has been shown in Ref. 8.

The effect of shape and AR on the heavy-hole band profile is much stronger, as can be seen in Fig. 3(b). For ellipsoidal dots, the energy within the dot is constant. As the AR is increased, the heavy-hole band within the dot moves up in energy, forming a deeper confinement for the holes. The increase in the confinement energy is as large as ≈200 meV when the AR changes from 1 to 8. One can also note that there are darker blue areas in the matrix near the interface, which are lower in energy than in the matrix away from the dot. This is due to the downward band bending, which increases the heavy-hole confinement even further. This feature is discussed in more detail later.

The light-hole band profile is shown in Fig. 3(c). Again, homogeneous color distribution within the ellipsoidal dot indicates constant energy. By comparing Figs. 3(b) and 3(c), one can see that the light-hole band is much lower in energy within the dot. In addition, the band-edge energy in the matrix near the interface is *higher* than it is away from the dot. This is due to the upward light-hole band bending near the interface. Because of this, the confinement potential for light holes is much shallower than that for heavy holes. Also, we note that the light-hole band profile does not change significantly with increasing AR.

The main difference in the strain distribution between the ellipsoidal and lens shapes is that in the later case, the strain is inhomogeneous across the dot. This results in a varying band profile across the dot. It is worth noting that the band edge is at the highest energy at the base of the dot for heavy holes and at the top of the dot for light holes. However, the overall variation in strain and hence in the band profile is relatively small as compared to the confinement energies. In general, all band profiles are very similar for both dot shapes, in agreement with our previous results.[8]

To show the variation in the band profile for the lens-shape dots in more detail, it is plotted in Fig. 4 along the [001] growth direction for several ARs. The overall variation in the band profile does not exceed 100 meV. The band profile for the lens shape becomes more homogeneous (and hence more similar to the ellipsoidal shape) with increasing aspect ratio. One can also notice that the heavy-hole band within the dot moves up in energy with increasing aspect ratio, while the light-hole energy within the dot is almost unchanged. The split-off valence band is also shown as an illustration. Within the dot, it moves down in energy with increasing AR, resulting in almost vanishing confinement potential at AR=8.

Note that Fig. 4(b) shows the band profile for AR=3.5. We performed calculations for this specific AR value in order to facilitate comparison with Ref. 1, in which the band structure was modeled for a variety of lens-shaped QD systems with AR≈3.5. Our results and those from Ref. 1 [indicated by arrows in Fig. 4(b)] are in excellent agreement.

Another important structural parameter of SAQDs is the dot composition. Now, we examine how the dot composition affects the strain-modified band profile, as even nominally pure InSb SAQDs may contain a significant percentage of As. Figure 5 shows the band profiles in $InAs_xSb_{1-x}$/InAs dots of ellipsoidal shape and with AR=2 for several compositions. For simplicity, we assume a homogeneous composition profile within the dot and neglect segregation into the matrix. The conduction-band edge in the dot shifts in energy with As composition, but this does not affect the ground electron state as it is not confined in the dot. However, the effect on the valence band is enormous. Both heavy- and light-hole bands move down in energy as the As percentage increases, significantly reducing the confinement potential. Note that the split-off valence band demonstrates an opposite

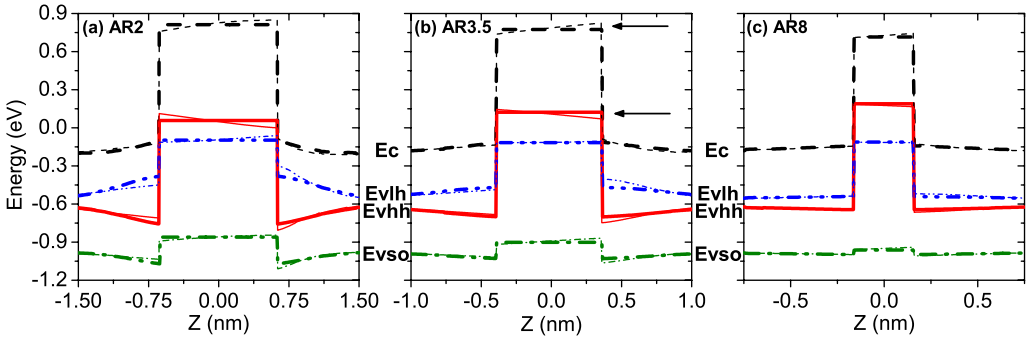

FIG. 4. (Color online) Strain-modified band profiles along the [001] growth direction through the dot center for ellipsoidal (thick lines) and lens (thin lines) SAQD shapes: Dashed line—conduction band, solid line—heavy-hole band, dash-dot-dot line—light-hole band, dash-dot line—split-off valence band. (a) AR=2; (b) AR=3.5; (c) AR=8. Short arrowhead lines in Fig. 4(b) indicate the averaged band-edge energies from Ref. 1 for lens-shaped dots of AR≈3.5

trend. It moves up in energy as the percentage of As increases, inducing a deeper confinement.

B. Energy levels

So far, we have discussed the effects of the structural parameters on the band profiles, which are size independent in the continuum-elasticity approximation. Now, we proceed to examining the single-particle electron and hole states, which are (of course) size dependent. In our calculations, we use a fixed value of the dot base size of 2.5 nm; i.e., varying the AR implies varying the dot height. Note that the base size is the only structural parameter of (very small) InSb/InAs SAQDs that can be experimentally measured with meaningful accuracy, and the value of 2.5 nm is close to experimental data reported in the literature.[5–7] We have modeled the electronic states only for the ellipsoidal dot because from the calculated band profile, we expect the effect of shape to be insignificant.

Figure 6(a) shows the single-particle electron and hole energy levels at 80 K as a function of the AR. Positions of the valence-band edges are also shown for reference. The position of the electron level remains almost constant. The heavy-hole band edge in the dot moves up in energy with AR. However, the size-quantized hole level demonstrates the opposite trend; the level is pushed down toward the heavy-hole band edge in the matrix with increasing AR. This demonstrates the dominant contribution from the size-quantization effect due to decreasing dot height.

The hole level is below the ground electron state for dots of 2.5 nm base, despite the broken-gap alignment of the band edges. The ground-state optical transition is due to recombination of weakly bound electrons in the matrix around the dot and holes strongly localized in the dot. Figure 6(b) shows the transition energies as a function of AR; results for both 80 and 300 K were obtained for comparison with experimental data.[5,6] The transition energy increases with increasing AR.

Note that the hole level in the dot is lower in energy than the electron level in the matrix because of the large size-quantization energy for holes (up to the dot size of 3.5 nm in diameter). This is intrinsically related to the small size of the dot (indeed for AR=1, the transition energy is expected to be as small as 100 meV); this may explain why no PL was observed from InSb/InAs dot of larger sizes as reported in Ref. 7.

For alloyed $InAs_xSb_{1-x}$/InAs QDs, we have performed calculations for a fixed AR=2, i.e., the base is 2.5 nm and the height is 1.25 nm. The single-particle energy levels as well as the transition energies are shown in Fig. 7 as a function of As composition. As shown in Fig. 7(a), the electron level remains constant and the heavy-hole level moves down in energy following the band-edge position. Figure 7(b)

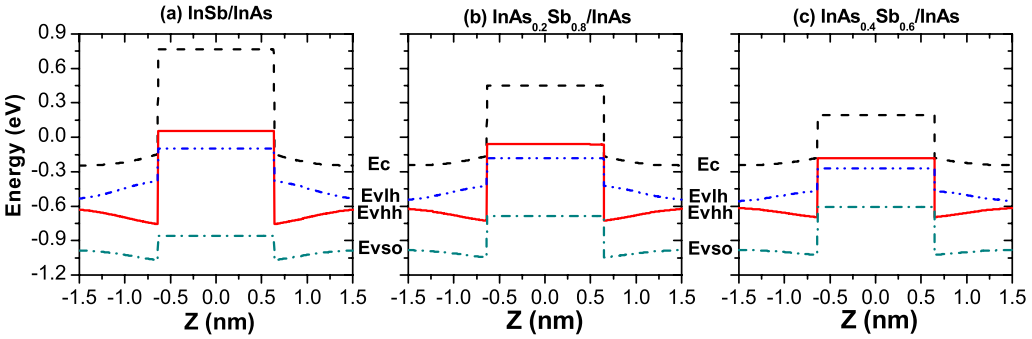

FIG. 5. (Color online) Strain-modified band profile for alloyed ellipsoidal $InAs_xSb_{1-x}$/InAs SAQDs of AR=2 for several As compositions. Dashed line—conduction band, solid line—heavy-hole band, dash-dot-dot line—light-hole band, dash-dot line—split-off valence band. (a) InSb/InAs; (b) $InAs_{0.2}Sb_{0.8}$/InAs; (c) $InAs_{0.4}Sb_{0.6}$/InAs.

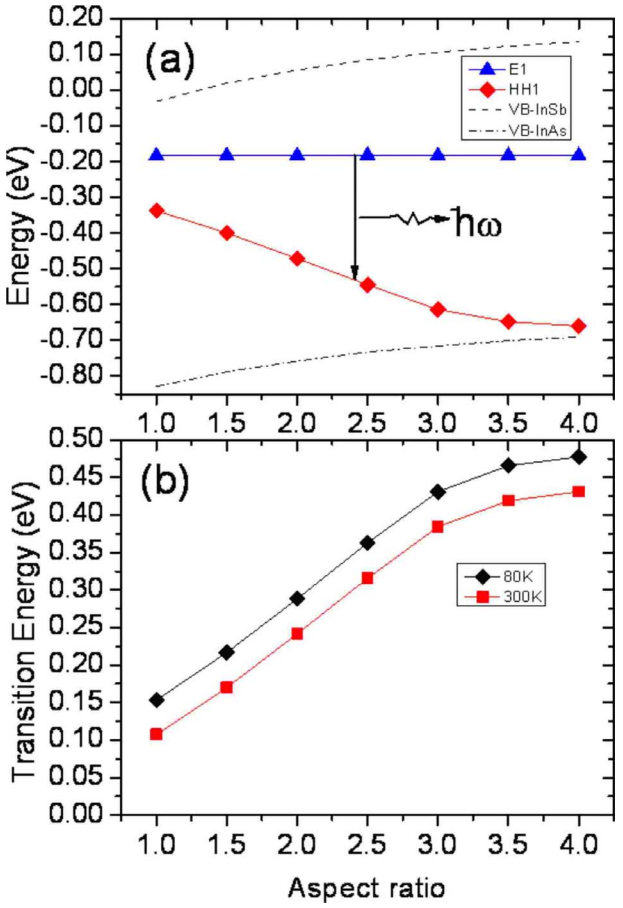

FIG. 6. (Color online) (a) Single-particle electron and hole energy levels (triangles and diamonds, respectively) as a function of the aspect ratio for pure InSb/InAs ellipsoidal SAQDs at 80 K. Dashed and dash-dot lines are InSb and InAs valence-band edges, respectively, shown for reference. (b) Ground-state transition energies at 80 and 300 K (diamonds and squares, respectively). Symbols represent calculated results; solid lines are guides for the eye.

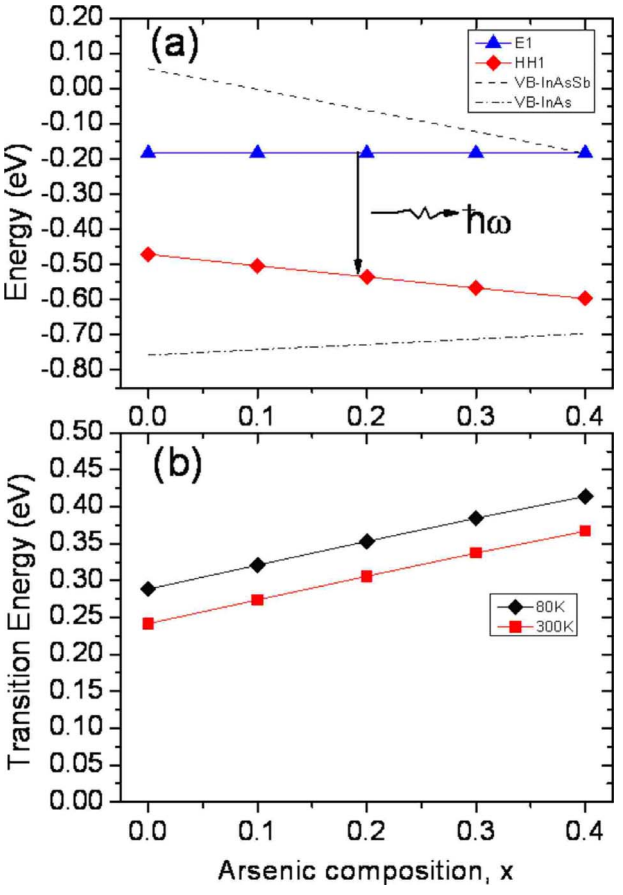

FIG. 7. (Color online) (a) Single-particle electron and hole energy levels (triangles and diamonds, respectively) as a function of composition x for $InAs_xSb_{1-x}$/InAs ellipsoidal SAQDs of AR=2 at 80 K. Dashed and dash-dot lines are InSb and InAs valence-band edges, respectively, shown for reference. (b) Ground-state transition energies at 80 and 300 K (diamonds and squares, respectively). Symbols represent calculated results; solid lines are guides for the eye.

shows how the transition energy increases with increasing As composition.

Now, we are in the position to illustrate how the structural parameters of the dots can be assessed from the optical data. For this, we compare our results with the reported experimental data. References 5 and 6 report PL from several InSb/InAs SAQD samples. At 80 K, the PL peaks are in the range of 0.33–0.36 eV. All samples exhibit bright PL at temperatures up to 300 K, redshifted to the range of 0.29–0.32 eV. The redshift is ≈40 meV, which agrees well with the value of ≈45 meV obtained from our calculations.

If we assume that the dots are pure InSb and the average lateral size is 2.5 nm,[5,6] the dot has to have an AR of 2.3–2.6 for the transitions to be within the reported range. As an example, an AR of ≈2.5 is needed for a transition energy of 0.34 eV at 80 K (and of 0.30 eV at 300 K), as indicated by the downward arrow in Fig. 6. On the other hand, if we find somehow that for the same dots, the AR=2 (rather than 2.5), we should expect a significant As alloying. In this case, the dot would be expected to contain as much as 20% As, indicated by the downward arrow in Fig. 7.

Although only ground-state transitions from InSb/InAs SAQDs have been reported,[5,6] it is worth mentioning that from our calculations, excited states for holes are also expected in this system. For the AR range under consideration, at least one excited hole state is expected. The separation between the levels should be about 140 meV. The separation between first and second excited states is found to be smaller, i.e., about 40 meV. For alloyed $InAs_xSb_{1-x}$/InAs SAQDs with AR=2, at least three excited states are expected.

Finally, we would like to comment on the relationship between PL intensity and dot size for this SAQD system, which originates from the type-II band alignment. The degree of penetration of the electron wave function into the dot and hence the electron-hole overlap integral are both strongly affected by the dot size; this is similar to W-type quantum-well structures.[4] Thus the oscillator strength for the PL transition is expected to decrease dramatically with increasing dot size. Indeed, our estimates show that the oscillator strength drops by more than an order of magnitude if the dot size increases from 2.5 to 10 nm. This provides another reason for the observed quenching of PL from larger InSb/InAs dots.[7]

The integrated intensity of the InSb-related PL peak at 300 K is reported to be about 15–20 times lower than that at 80 K. This is in agreement with deep localization of holes in the dot; in addition, it indicates a relatively low level of nonradiative recombination.

IV. CONCLUSIONS

We have modeled the electronic structure of $InAs_xSb_{1-x}$/InAs SAQDs of various shapes, aspect ratios, and compositions using strain-dependent multiband $\boldsymbol{k}\cdot\boldsymbol{p}$ theory. $InAs_xSb_{1-x}$/InAs SAQDs exhibit a type-II broken-gap alignment. Our analysis shows that strong confinement exists for holes only, with electrons loosely bound around the dot. The hole confinement potential is not sensitive to details of the dot shape and is essentially defined only by the dot aspect ratio.

With increasing aspect ratio, strain-induced splitting of valence band increases, and a deeper confinement is formed. However, for a fixed lateral size, the optical transition energy increases with the aspect ratio as a result of the dominant contribution of the size-quantization effect. The effect of variation in the dot composition is comparable to that of aspect ratio on the hole levels. Hence, the $InAs_xSb_{1-x}$/InAs SAQD system provides wide-ranging possibilities for band-gap engineering in the midinfrared range.

Our calculations show that structural parameters of the dots can be estimated using the optical spectra.

ACKNOWLEDGMENTS

This work was supported by the European Commission Grant No. FP6–017393 DOMINO.

*g.yeap@2004.hull.ac.uk

[1] C. E. Pryor and M.-E. Pistol, Phys. Rev. B **72**, 205311 (2005).
[2] S. I. Rybchenko, G. H. Yeap, R. Gupta, I. E. Itskevich, and S. K. Haywood, The Eighth International Conference on Mid-Infrared Optoelectronics: Materials and Devices, Bad Ischl, 2007 (unpublished).
[3] S. I. Rybchenko, R. Gupta, K. T. Lai, I. E. Itskevich, S. K. Haywood, V. Tasco, N. Deguffroy, A. N. Baranov, and E. Tournié, Phys. Rev. B **76**, 193309 (2007).
[4] J. R. Meyer, C. A. Hoffman, F. J. Bartoli, and L. R. Ram-Mohan, Appl. Phys. Lett. **67**, 757 (1995).
[5] S. V. Ivanov, A. N. Semenov, V. A. Solov'ev, O. G. Lyublinskaya, Ya. V. Terent'ev, B. Ya. Meltser, L. G. Prokopova, A. A. Sitnikova, A. A. Usikova, A. A. Toropov, and P. S. Kop'ev, J. Cryst. Growth **278**, 72 (2005).
[6] V. A. Solov'ev, O. G. Lyublinskaya, A. N. Semenov, B. Ya. Meltser, D. D. Solnyshkov, Ya. V. Terent'ev, L. A. Prokopova, A. A. Toropov, S. V. Ivanov, and P. S. Kop'ev, Appl. Phys. Lett. **86**, 011109 (2005).
[7] O. G. Lyublinskaya, V. A. Solov'ev, A. N. Semenov, B. Ya. Meltser, Ya. V. Terent'ev, L. A. Prokopova, A. A. Toropov, A. A. Sitnikova, O. V. Rykhova, and S. V. Ivanov, J. Appl. Phys. **99**, 093517 (2006).
[8] S. I. Rybchenko, G. Yeap, R. Gupta, I. E. Itskevich, and S. K. Haywood, J. Appl. Phys. **102**, 013706 (2007).
[9] I. Vurgaftman, L. R. Ram-Mohan, and J. R. Meyer, J. Appl. Phys. **89**, 5815 (2001).
[10] J. D. Eshelby, in *Solid State Phys.*, edited by F. Seitz and D. Turnbull (Academic, New York, 1956), Vol. 3, p. 79; Proc. R. Soc. London, Ser. A **241**, 376 (1957).
[11] H. Jiang and J. Singh, Phys. Rev. B **56**, 4696 (1997); IEEE J. Quantum Electron. **34**, 1188 (1998).
[12] A. J. Williamson, L. W. Wang, and A. Zunger, Phys. Rev. B **62**, 12963 (2000); L. W. Wang and A. Zunger, *ibid.* **59**, 15806 (1999); L. W. Wang, J. Kim, and A. Zunger, *ibid.* **59**, 5678 (1999).
[13] S. Lee, F. Oyafuso, P. von Allmen, and G. Klimeck, Phys. Rev. B **69**, 045316 (2004); S. Lee, O. L. Lazarenkova, P. von Allmen, F. Oyafuso, and G. Klimeck, *ibid.* **70**, 125307 (2004).
[14] M. A. Cusack, P. R. Briddon, and M. Jaros, Phys. Rev. B **54**, R2300 (1996).
[15] C. Pryor, Phys. Rev. B **57**, 7190 (1998).
[16] M. Grundmann, O. Stier, and D. Bimberg, Phys. Rev. B **52**, 11969 (1995).
[17] G. R. Liu and Q. Jerry, Semicond. Sci. Technol. **17**, 630 (2002).
[18] W. Lee, J.-M. Myong, Y.-H. Yoo, and H. Shin, Solid State Commun. **132**, 135 (2004).
[19] G. Muralidharan, Jpn. J. Appl. Phys., Part 2 **39**, L658 (2000).
[20] M. Tadic, F. M. Peeters, K. L. Janssens, M. Korkusinski, and P. Hawrylak, J. Appl. Phys. **92**, 5819 (2002).
[21] M. K. Kuo, T. R. Lin, B. T. Liao, and C. H. Yu, Physica E **26**, 199 (2005).
[22] A. Carlsson, L. R. Wallenberg, C. Persson, and W. Seifert, Surf. Sci. **406**, 48 (1998).
[23] T. Benabbas, P. Francois, Y. Androussi, and A. Lefebvre, J. Appl. Phys. **80**, 2763 (1996).
[24] S.-H. Wei and A. Zunger, Phys. Rev. B **49**, 14337 (1994).
[25] S. L. Chuang, *Physics of Optoelectronic Devices* (Wiley, New York, 1995).
[26] S.-H. Park, D. Ahn, and Y.-T. Lee, J. Appl. Phys. **96**, 2055 (2004).
[27] C. Pryor, M.-E. Pistol, and L. Samuelson, Phys. Rev. B **56**, 10404 (1997).
[28] T. B. Bahder, Phys. Rev. B **45**, 1629 (1992); **41**, 11992 (1990).
[29] J. Los, A. Fasolino, and A. Catellani, Phys. Rev. B **53**, 4630 (1996).
[30] B. A. Foreman, Phys. Rev. B **56**, R12748 (1997).
[31] F. Boxberg and J. Tulkki, Rep. Prog. Phys. **70**, 1425 (2007).